Three-dimensional investigation of thermal barrier coatings by synchrotron-radiation computed laminography

V. Maurel,[a,*] L. Helfen,[b] F. N'Guyen,[a] A. Koster,[a] M. Di Michiel,[c] T. Baumbach[b] and T.F. Morgeneyer[a]

[a]Centre des Matériaux, Mines ParisTech, UMR CNRS 7633, BP 87, F-91003 Evry Cedex, France
[b]Institut fur Synchrotronstrahlung (ISS/ANKA), Forschungszentrum Karlsruhe, D-76344 Eggenstein-Leopoldshafen, Germany
[c]European Synchrotron Radiation Facility, F-38043 Grenoble Cedex 9, France

Characterization of the microstructure of thermal barrier coatings (TBCs) is essential for assessing coating lifetime and for understanding the damage mechanisms leading to ceramic layer spallation. Recent progress in synchrotron-radiation computed laminography (SRCL) enables imaging of samples that are thin but extended in two dimensions. This study reports on the first results of the 3-D characterization of electron beam–physical vapour deposition TBCs by SRCL. Image analysis was very helpful in investigating the 3-D microstructure obtained and is also described.
© 2011 Acta Materialia Inc. Published by Elsevier Ltd. All rights reserved.

Keywords: EB-PVD thermal barrier coating; X-ray synchrotron-radiation computed laminography; Bond-coat microstructure; 3-D image analysis

Thermal barrier coatings (TBCs) are often used for thermal insulation and as a passivation system for hot components for industrial applications [1]. TBCs are multilayered systems. A ceramic top-coat layer is interfaced with the substrate via a bond-coat layer. The latter is used as an aluminium reservoir to create an adherent and stable interfacial α-alumina layer, comprising thermally grown oxide (TGO), between the ceramic top-coat layer and the metallic bond-coat layer [1]. Interfacial damage can occur and assessment of the lifetime of these systems is critical as ceramic breakaway leads to the loss of substrate protection and damage of the component at high temperatures [1–3].

The final breakaway of TBC is known to be triggered by delamination of the ceramic/bond-coat interface [3,4]. Thus, characterization of TBC microstructure and observation of its evolution is essential for assessing coating lifetime and for understanding the damage mechanisms leading to ceramic layer spallation. Moreover, the 3-D microstructure morphology is known to have an effect on local stress and strain fields resulting in interfacial delamination.

Unfortunately, most classical metallography specimen preparation techniques, including machining, polishing, electrodischarge machining and focused ion beam milling are known to introduce artefacts in the microstructure and confuse subsequent observations. Interfacial cracks as well as ceramic layer spallation might even be induced by these preparation techniques with few means being available to determine the true cause of damage. Synchrotron-radiation computed tomography (SRCT) offers an interesting way of determining the cause of debonding. The technique is very attractive for 3-D microstructure analysis for an increasing variety of materials [5]. However, computed tomography (CT) requires coupons of very small diameter so as to ensure X-ray illumination and projection to the detector of the entire volume for all angular projections (to avoid unreliable or truncated projection data). This point is particularly critical when using Ni-base material for the coated substrate and would also make it difficult to machine the coupon without inducing damage. The technique of synchrotron-radiation computed laminography (SRCL) [6] enables the scanning of samples that are still thin but extended in two dimensions. For stick-like material samples, the technique has been shown to yield results only slightly inferior to those obtained by SRCT [7] which is due to incomplete sampling of the specimen's 3-D Fourier domain. For thin plate-like specimens, however, the method is able to show much better results than SRCT [8,9] since projection angles with the specimen's long side oriented parallel to the beam direction are avoided. SRCL observation of in situ damage evolution in thin sheet material has

---

*Corresponding author. E-mail: vincent.maurel@mat.ensmp.fr

successfully been applied to Al alloys [10] and fibre epoxy composites [7]. It has already been demonstrated that in combination with high-energy synchrotron radiation the technique is able to penetrate and image highly absorbing specimens [11–14]. Moreover, compared to its laboratory counterparts [15], the technique can significantly benefit from phase contrast, highlighting the interfaces between different materials [16–18]. Thus this technique seems to be a perfect candidate for the high-resolution investigation of thin layered systems, such as TBCs, avoiding the creation of artefacts linked to the preparation of the specimen.

This study reports on the first results of the 3-D characterization of electron beam–physical vapour deposition (EB-PVD) TBCs by SRCL. Image analysis was very helpful in investigating the 3-D microstructure obtained and will be also described.

The TBC system used in this study was processed by the Ceramic Coating Centre (CCC) and the Snecma–Safran Group. The substrate material was a Ni-based single-crystal superalloy AM1, the composition of which is detailed in Table 1. The bond-coat was a Pt-enriched aluminide overlayer (Ni,Pt)Al deposited by pack-cementation. The outer layer was mostly composed of betaphase NiAl, the composition of which is detailed in Table 2. The ceramic layer was an EB-PVD Y_2O_3 partially stabilized zirconia coating 150 μm thick. Hollow cylindrical test specimens were used for this study to reduce thermal inertia during heating or cooling. The substrate outer diameter was 11 mm within the gauge length and 1 mm in thickness. Each specimen was first cut into a small cylinder of 8 mm length. Then, it was sliced using a diamond string saw to extract the coupon to be examined. The final dimensions of the coupon were 500 μm for the maximum thickness and 8 mm in length. No further machining was necessary before SRCL scanning.

Before SRCL observation and specimen machining, 32 thermal cycles of 1 h were performed at 1100 °C. The cooling and heating rates were 5 °C s^{-1}. The TGO average thickness was found to be 1.6 μm from scanning electron microscopy (SEM) analysis of a given cross-section.

SRCL [9] was used in this study. The technique is basically similar to SRCT [8] except that the sample was imaged under rotation around an axis which was inclined by $\theta = 60°$ with respect to the beam (where $\theta = 90°$ for CT). For planar samples this ensures that the X-ray transmission is relatively constant at each incremental angle and allows large samples to be imaged locally at high resolution [9] without the need for samples containing the regions of interest (ROIs) to be physically extracted. Details about the principles and the reconstruction procedure can be found in Refs. [8,17,9]. Imaging was performed at beam line ID15 of the ESRF using a polychromatic X-ray beam with energies between approximately 30 and 65 keV. Radiographs at different projection angles of the specimen were acquired with 100 ms exposure time. Volumes were reconstructed using an in-house software package from 1500 of such angularly equidistant projection radiographs over a specimen rotation angle of 360°. The size of the volume analysed was $800 \times 800 \times 1000$ voxels with a voxel size of $0.84 \times 0.84 \times 0.84$ μm^3. The ROI was centred in the coupon, leading to a minimum distance between the edge of the coupon and the edge of the ROI of 1.5 mm.

A representative reconstructed pseudo-3-D view of SRCL data of the specimen is shown in Figure 1. An arbitrary reference plane, $z = 0$, was associated approximately with the interface between the bond-coat layer and the interdiffusion zone (IDZ) (Fig. 2). In Figure 1, the plane $z = 11$ μm was located in the bond-coat layer where segregation of impurities at the bond-coat grain boundaries was assumed to be the origin of the absorption contrast obtained. The plane $z = 85$ μm was located in the ceramic layer where voids induced by the EB-PVD process and the columnar structures of the ceramic layer were the essential sources of contrast. Associated cross-sections, e.g. in xz and yz planes, respectively, revealed the columnar structures of the ceramic layer and the location of the TGO layer (Fig. 1 and Fig. 2). At the bond-coat/ceramic interface dark areas were assumed to be related to TGO and interfacial voids. This point will be discussed below. As a first result, the homogeneity of the information over the whole 3-D scan ensured that no edge effect should occur as a result of either specimen preparation and SRCL techniques.

A simple grey value thresholding technique was not able to extract either grains or ceramic columns from the images due to the contrast obtained and average grey level variations through the scan. Local grey value minima were therefore used to extract geodesic markers from the 3-D images [19], e.g. in the bond-coat layer (Fig. 3a). Nevertheless, a distinction should be made between geodesic markers within a grain and those located at the grain boundary. This step was performed using watershed segmentation in order to construct grain boundaries in 3-D (see Fig. 3b) [19–21].

260 grains have been reconstructed in the bond-coat layer with an average volume of 1.4×10^5 μm^3 and an apparent diameter of 38 μm that was confirmed using the intercept method for the middle plane extracted from the bond-coat layer. The obtained grain size was seen to be consistent with the grain size of the bond-coat layer previously identified for this material, when SEM was used to observe the cross-section as well as for in-plane analysis with or without electron backscatter diffraction measurement [22,4].

The image analysis methodology detailed above for the bond-coat layer was applied for analysis of the ceramic layer. Thus packs of sintered ceramic columns have been segmented in 3-D (Fig. 3c).

The ceramic/bond-coat interface is physically defined by the TGO layer. Nevertheless, the spatial resolution of the SRCL was, for the specimen studied, similar to the TGO thickness, making direct detection of the TGO layer difficult. To extract with a maximum of confidence the 3-D ceramic/bond-coat interface, data related to local minima should be associated with the bottom of the ceramic columns. Local grey level minima as well as the bottom of the ceramic columns were used to construct a 3-D interface based on a 3-D spline function algorithm (Fig. 4a). The measured ratio between total surface of the 3-D ceramic/bond-coat interface, S, projected onto the reference plane, S_0, is equal to 1.42 for the whole volume analysed. This ratio, as well as the wavy form obtained of the 3-D ceramic/bond-coat interface, were

Table 1. Chemical composition (in wt.%) of single-crystal Ni-base superalloy AM1 at room temperature [24].

	Ni	Co	Cr	Mo	W	Ta	Al	Ti	C	Fe	S
Min	Bal.	6	7	1.8	5	7.5	5.1	1			3 ppm
Max	Bal.	7	8	2.2	6	8.5	5.5	1.4	0.01	0.2	

Table 2. Chemical composition (in at.%) of Ni(Pt,Al) bond-coat layer in the as-received condition [25].

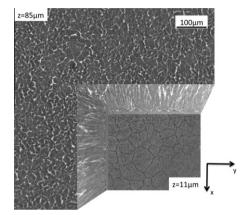| Al	Pt	Cr	Co	Ni	Ti	Ta	Mo	W
35.2	7.3	1.0	4.6	42.0	0	1.0	0	0

Figure 1. Reconstruction of the studied TBC via 3-D SRCL. Top plane ($z = 85$ μm) is located within the ceramic layer. An arbitrary virtual cut was made to show a plane ($z = 11$ μm) located within the bond-coat layer and two orthogonal cross-sections. The ordinate reference corresponds to Fig. 2.
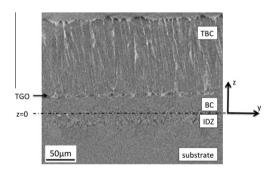

Figure 2. Cross-section of the studied TBC obtained by 3-D SRCL. The reference plane used corresponds approximately to the interface between the bond-coat layer and the interdiffusion zone (IDZ).

seen to be consistent with the TBC cross-sections or surface measurements without ceramic top-coat found in the literature [23].

Moreover, the intersection of bond-coat grains and of the 3-D ceramic/bond-coat interface has led to a very satisfying description of the bond-coat layer (Fig. 4b). Local minima associated with a low grey level, close to the ceramic/bond-coat 3-D interface, might be associated with both interfacial voids and local higher TGO thickness (Fig. 4b). Because this distinction was ambiguous, those local minima close to the ceramic/bond-coat 3-D interface will here be considered as interfacial defects in the following. To analyse only TGO defects or interfacial voids, local minima were selected when exceeding 2 μm³ (Fig. 4b).

Qualitatively, when the interfacial defects were examined through the thickness of the specimen, it was found that most of these defects were correlated to the local growth orientation of ceramic columns as well as local cracks at the bottom of the columns. This assessment was carried out by comparing voids extracted on each cross-section together with a 3-D reconstruction of packs of sintered ceramic columns (Fig. 3c).

In the same way, by examining each cross-section at every depth, together with the 3-D reconstruction (see Fig. 4b), some interfacial defects were found to be correlated with the grain-boundary network of the bond-coat layer and especially with triple junction points. It should be noted that this last point could not be revealed without a complete-3D technique such as is presented here. This methodology could be a route to determine the way voids or the TGO grow at the bond-coat/ceramic interface. Indeed a distinction could be made between defects related to the bond-coat grain boundary network and those related to the EB-PVD process. Thus for the specimen studied, it could be assumed that grain-boundary diffusion has modified the microstructure morphology. With a longer
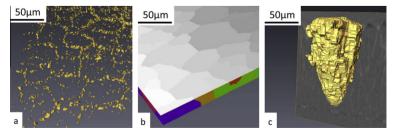

Figure 3. Image analysis results from the reconstructed 3-D volume: (a) geodesic markers, associated to local grey-level minima of 3-D images, used to define bond-coat grain boundaries; (b) 3-D grains obtained from image reconstruction in the bond-coat; (c) 3-D pack of sintered columns obtained from image reconstruction in the ceramic layer.
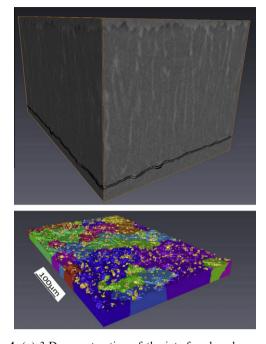
Figure 4. (a) 3-D reconstruction of the interface based on geodesic markers and 3-D ceramic column shape. Interface is in black. (b) Bond-coat layer and interfacial defects. Defects are highlighted in gold, bond-coat grains are in colour. (For interpretation of the references to colour in this figure legend, the reader is referred to the web version of this article.)

time spent at high temperature, it could be expected that the TGO thickness and roughness would be sufficient to increase the contrast of the images. Thus the exact location and thickness of the TGO layer would be more easily determined.

This study has shown the possibility of using SRCL for investigating, for the first time, a 3-D TBC microstructure. The first benefit of the methodology was seen in the way it limits the artefacts inherent in the traditional specimen preparation methods, by observing an area far away from the edge of the specimen. This step was validated by the homogeneity of the microstructure in the volume observed. Using image analysis and 3-D reconstruction has allowed major microstructural features to be identified in the TBC systems: bond-coat grains and associated grain-boundaries, ceramic columns and sintered columns and interfacial defects located at the bond-coat/ceramic interface. It is worth noting that despite a coarse spatial resolution compared to the TGO thickness, the ceramic/bond-coat interface was determined in 3-D with a very satisfying accuracy. Thus this study highlights a very promising way to understand the microstructure and especially the evolution of the morphology which is known to be among the main features responsible for damage in TBC systems.

[1] A.G. Evans, D.R. Mumm, J.W. Hutchinson, G.H. Meier, F.S. Pettit, Prog. Mater. Sci. 46 (5) (2001) 505–553, <http://www.sciencedirect.com/science/article/B6TX1-4372WDK-2/2/528639fddb36aca05a09a653d333d3b2>.

[2] P. Wright, A. Evans, Curr. Opin. Solid State Mater. Sci. 4 (3) (1999) 255–265, <http://www.sciencedirect.com/science/article/pii/S1359028699000248>.

[3] N. Yanar, F. Pettit, G. Meier, Metall. Mater. Trans. A 37 (5) (2006) 1563–1580, <http://dx.doi.org/10.1007/s11661-006-0100-4>.

[4] C. Courcier, V. Maurel, L. Rémy, S. Quilici, I. Rouzou, A. Phelippeau, Surf. Coatings Technol. 205 (13-14) (2011) 3763–3773, <http://www.sciencedirect.com/science/article/B6TVV-51Y57FC-4/2/d26ec16a1de5b850aa59dce80eaa469c>.

[5] T.F. Morgeneyer, J. Besson, Scripta Mater. 65 (11) (2011) 1002–1005, <http://www.sciencedirect.com/science/article/pii/S1359646211005306>.

[6] L. Helfen, T. Baumbach, P. Mikulík, D. Kiel, P. Pernot, P. Cloetens, J. Baruchel, Appl. Phys. Lett. 86 (2005) 071915.

[7] A. Moffat, P. Wright, L. Helfen, T. Baumbach, G. Johnson, S. Spearing, I. Sinclair, Scripta Mater. 62 (2) (2010) 97–100, <http://www.sciencedirect.com/science/article/pii/S1359646209005983>.

[8] L. Helfen, T. Baumbach, P. Pernot, P. Mikulík, M. DiMichiel, J. Baruchel, Proc. SPIE 6318 (2006) 63180 N.

[9] L. Helfen, A. Myagotin, P. Mikulík, P. Pernot, A. Voropaev, M. Elyyan, M.D. Michiel, J. Baruchel, T. Baumbach, Rev. Sci. Instrum. 82 (6) (2011) 063702, <http://link.aip.org/link/?RSI/82/063702/1>.

[10] T.F. Morgeneyer, L. Helfen, I. Sinclair, H. Proudhon, F. Xu, T. Baumbach, Scripta Mater. 65 (11) (2011) 1010–1013, <http://www.sciencedirect.com/science/article/pii/S1359646211005318>.

[11] L. Helfen, A. Myagotin, P. Pernot, M. DiMichiel, P. Mikulík, A. Berthold, T. Baumbach, Nucl. Inst. Meth. A 563 (2006) 163–166.

[12] L. Helfen, A. Myagotin, A. Rack, P. Pernot, P. Mikulík, M.D. Michiel, T. Baumbach, Phys. Stat. Sol. (a) 204 (2007) 2760–2765.

[13] A. Houssaye, F. Xu, L. Helfen, V.D. Buffrénil, T. Baumbach, P. Tafforeau, J. Vert. Paleontol. 31 (2011) 2–7.

[14] T. Tian, F. Xu, J. Han, D. Choi, Y. Cheng, L. Helfen, M.D. Michiel, T. Baumbach, K. Tu, Appl. Phys. Lett. 99 (2011) 082114.

[15] S. Gondrom, J. Zhou, M. Maisl, H. Reiter, M. Kröning, W. Arnold, Nucl. Eng. Des. 190 (1999) 141–147.

[16] K. Krug, L. Porra, P. Coan, A. Wallert, J. Dik, A. Coerdt, A. Bravin, M. Elyyan, P. Reischig, L. Helfen, T. Baumbach, J. Synchrotron Rad. 15 (2008) 55–61.

[17] L. Helfen, T. Baumbach, P. Cloetens, J. Baruchel, Appl. Phys. Lett. 94 (2009) 104103.

[18] F. Xu, L. Helfen, A.J. Moffat, G. Johnson, I. Sinclair, T. Baumbach, J. Synchrotron Rad. 17 (2010) 222–226.

[19] J. Serra, L. Vincent, Circuits Syst. Signal Process. 11 (1) (1992) 47–108.

[20] C. Lantuejoul, S. Beucher, J. Microsc. Oxford 121 (Jan) (1981) 39–49.

[21] J. Crespo, J. Serra, R. Schafer, Signal Process. 47 (2) (1995) 201–225.

[22] V. Maurel, M. Harvey, L. Rémy, Surf. Coatings Technol. 205 (10) (2011) 3158–3166, <http://www.sciencedirect.com/science/article/B6TVV-51H1DBV-3/2/2528627fcc34f6403c84d373e3174478>.

[23] S. Dryepondt, D.R. Clarke, Acta Mater. 57 (7) (2009) 2321–2327, <http://www.sciencedirect.com/science/article/B6TW8-4VR6PX8-3/2/9b6490b831d699d71616d7520e8eba0a>.

[24] R. Molins, C. Guerre, L. Rémy, Rev. Métall.-CIT/Sci. Génie des Matériaux (2003) 507–512.

[25] C. Guerre, R. Molins, L. Rémy, Mater. High Temp. 17 (2) (2000) 197–203.